Journal of Magnetism and Magnetic Materials 535 (2021) 168095

Contents lists available at ScienceDirect

Journal of Magnetism and Magnetic Materials

journal homepage: www.elsevier.com/locate/jmmm

Research articles

Exploring the magnetic properties and magnetic coupling in $SrFe_{12}O_{19}$/$Co_{1-x}Zn_xFe_2O_4$ nanocomposites

P. Maltoni [a,*], T. Sarkar [a], G. Barucca [b], G. Varvaro [c], D. Peddis [c,d,*], R. Mathieu [a,*]

[a] Department of Materials Science and Engineering, Uppsala University, Box 35, SE-751 03 Uppsala, Sweden
[b] Università Politecnica delle Marche SIMAU, Via Brecce Bianche 12, 60131 Ancona, Italy
[c] Institute of Structure of Matter, Italian National Research Council (CNR), 00015 Monterotondo Scalo, Rome, Italy
[d] Dipartimento di Chimica e Chimica Industriale, Università di Genova, Via Dodecaneso 31, I-16146 Genova, Italy

ARTICLE INFO

Keywords:
Ferrites
Magnetic nanocomposites
Nanostructures

ABSTRACT

Among hard/soft nanocomposites (NCs), ferrite-based materials are potentially promising for developing exchange-coupled systems, thus leading to enhanced magnetic properties. In this regard, we investigate the role of the synthesis approach in the development of $SrFe_{12}O_{19}/CoFe_2O_4$ (SFO/CFO) NCs, with special focus on tuning the magnetic features of the softer phase (CFO) by introducing Zn^{2+} in the spinel structure. X-ray powder diffraction (XRPD), transmission electron microscopy (TEM) and squid magnetometry were employed to clarify the relationship between morphology, size, and magnetic properties of the NCs, pointing out the feasibility of this method in obtaining successfully exchange-coupled systems. This work shows how optimizing the intrinsic magnetic properties of the CFO may be used to tune the extrinsic ones of the NCs. Despite the promising results in magnetic coupling, our study clearly confirms/strengthens that an enhancement of remanent magnetization is the most important factor for improving the magnetic performance.

1. Introduction

The design of hard/soft bi-magnetic nanocomposites (NCs) have gained increasing attention in recent years and challenged the scientific community. Indeed, these systems offer the possibility of widely tuning their magnetic properties (i.e. magnetic anisotropy, saturation magnetization) at the nanoscale [1,2], as they are composed of two different ferro- or ferrimagnetic phases, with different extrinsic magnetic properties: a hard phase, with a high coercivity (H_C), and a soft one, with both a high saturation and remanent magnetization (M_S and M_R) [3]. If exchange-coupling interaction occurs, such a combination shall result in a material with both enhanced coercivity and magnetization, thus leading to improved energy products $(BH)_{MAX}$. This quantity describes the maximum amount of magnetic energy that can be stored in a magnet [4,5]. In fact, the novel magnetic interaction among the two phases at the interface may promote a significant enhancement of the remanence of the NC with only a small deterioration of the coercivity due to the introduction of a soft phase [1,6]. To achieve this goal, it is essential to tightly control the morpho-structural features of both the phases and maximize their interfacial contact. In this regard, ferrite-based composites have shown to be promising in the field of permanent magnets (PMs), especially M−type $SrFe_{12}O_{19}$/spinel MFe_2O_4 (M: Co, Zn, Ni, Mn), owing to the potential magnetic performance (energy products of 40–460 kJ m^{-3}) of the hexagonal ferrite and the flexible crystal structure of the spinel ferrite, offering many possibilities to modulate the magnetic anisotropy and saturation magnetization [7–11]. Nevertheless, the lack of comprehensive studies in literature on the degree of magnetic coupling in such systems is rather limited, thus leading to the need of thoroughly investigating the complex magnetic interactions bringing it forth. Various studies on ferrite-based NCs are reported in literature, dealing mainly with composites prepared as powders by physical mixing of the two phases or different chemical one-pot synthesis [11–13], which clearly show the challenges in obtaining an efficient exchange-coupling related to the synthetic approach. In our recent studies, we have addressed the role of synthesis strategy in controlling the magnetic coupling in bi-magnetic composites, thus showing that is possible to use sol–gel technique as an easy, scalable, low-cost and green synthesis method to produce tightly coupled NCs [14–18]. In this work, we first have explored a possible way to modify the extrinsic magnetic properties at the nanoscale of a hard $SrFe_{12}O_{19}$ (SFO) phase (anisotropy

* Corresponding authors at: Department of Materials Science and Engineering, Uppsala University, Box 35, SE-751 03 Uppsala, Sweden (P. Maltoni and R. Mathieu); Institute of Structure of Matter, Italian National Research Council (CNR), 00015 Monterotondo Scalo, Rome, Italy (D. Peddis).
E-mail addresses: pierfrancesco.maltoni@angstrom.uu.se (P. Maltoni), davide.peddis@unige.it (D. Peddis), roland.mathieu@angstrom.uu.se (R. Mathieu).

https://doi.org/10.1016/j.jmmm.2021.168095
Received 31 December 2020; Received in revised form 19 March 2021; Accepted 1 May 2021
Available online 9 May 2021

constant $K = 0.35$ MJ/m^3, $M_S \sim 0.38$ MA/m) introducing a softer $CoFe_2O_4$ (CFO) phase with a higher bulk $M_S \sim 0.45$ MA/m and lower anisotropy ($K = 0.29$ MJ/m^3) [5,19]. We use SFO/CFO 80/20 w/w % as the parent material and show the feasibility of introducing Zn^{2+} cations into the spinel structure of CFO using the above mentioned one-pot synthesis method. Zinc was chosen to increase the softness of the spinel CFO, lowering H_C and increasing M_S by substituting Co^{2+} with Zn^{2+} [7,20]. The effect of Zn^{2+} substitution on the extrinsic properties of the exchange-coupled NC is investigated. Our goal is to optimize the magnetic properties of such NCs by atomic structuring and modification of the intrinsic characteristics of CFO [21], and prove the feasibility of the one-pot synthesis method to design and obtain strongly coupled NCs with an overall good control on the crystallite sizes and homogeneous distribution even in the presence of an additional dopant (Zn). Therefore, we prepared three different NCs by substituting Co^{2+} in $Co_{1-x}Zn_xFe_2O_4$ with an increasing amount of Zn^{2+} (with x = 0.1, 0.3, 0.5, nominally): indeed, spinel ferriteś versatile crystal structure offers many possibilities to modulate the magnetic anisotropy, due to the rearrangement of cationic distribution among the tetrahedral (T_d) and Octahedral (O_h) sites, by chemical engineering [20,22,23]. Our study reveals that optimizing the magnetic properties of each single component of the NC is fundamental to achieve exchange coupled nanostructures with enhanced magnetic performances. It is important to note here that the change in H_C of the NCs can be a direct result of the Zn-doping and hence, an intrinsic effect on the anisotropy of CFO, but it can also have extrinsic contributions like the coupling between the two phases and the resulting change in the reversal process.

2. Synthesis and characterization

To prepare various hard/soft SFO/CFO nanocomposites (NCs), with composition 80/20 w/w %, a one-pot sol–gel route was used, described elsewhere [18,24]: briefly, two separate sols were first prepared by dissolving the precursors of SFO i.e., $Fe(NO_3)_3{\cdot}9H_2O$ and $Sr(NO_3)_2$ (Sigma-Aldrich) in a $[Fe^{3+}]/[Sr^{2+}]$ ratio of 11 (note that the initial non-stoichiometric starting ratio between Fe and Sr with a slightly higher presence of Sr enables the formation of SFO at lower temperatures [18]), and the precursors of CFO i.e., $Co(NO_3)_2{\cdot}6H_2O$ and $Fe(NO_3)_3{\cdot}9H_2O$ (Sigma-Aldrich) in a $[Fe^{3+}]/[Co^{2+}]$ ratio of 2 in deionized water Then a 1 M citric acid aqueous solution was added (molar ratio of total metals to citric acid 1:1), the dispersions were mixed together and the pH was adjusted to 7 by adding dropwise NH_3 (30%) (Sigma-Aldrich). Next, it was heated on a hot plate to 80 °C to form a dry gel, and the temperature was increased to 300 °C inducing a self-combustion. The obtained dry powders were ground and annealed at 950 °C for 3 h in air. We refer to this sample as NC. To evaluate the effect of magnetic anisotropy, three $SrFe_{12}O_{19}/Co_{1-x}Zn_xFe_2O_4$ (NC_s_Zn) samples were synthesized through this one-pot approach, using the same procedure as NC, however by substituting Co^{2+} with Zn^{2+}(keeping constant Fe^{3+}) with x: 0.1–0.3–0.5. We refer to these in the rest of the article as NC_Zn01, NC_Zn03, and NC_Zn05.

The final composition was confirmed by means of inductively coupled plasma optical emission spectroscopy (ICP–OES), carried out for elemental analysis with an iCAP 6300 DUP ICP–OES spectrometer (ThermoScientific) (see Table 1). A first check to verify the presence of organic molecules (residuals from the gel) on the final samples was done by means of Fourier-transform infrared spectroscopy (FTIR): the spectra were acquired with a Shimadzu IRPrestige-21, equipped with a Specac Golden Gate Single Reflection Diamond Attenuated total reflection (ATR). All samples were analyzed in the region between 4000 cm^{-1} and 400 cm^{-1}.

Table 1
List of samples, nominal composition and x: Zn content obtained from ICP analysis.

Id	Composition (80/20 (w/w %))	x ICP ($Co_{1-x}Zn_xFe_2O_4$)	Synthesis Method
NC	$SrFe_{12}O_{19}/CoFe_2O_4$	–	One pot sol–gel
NC_Zn01	$SrFe_{12}O_{19}/Co_{0.9}Zn_{0.1}Fe_2O_4$	0.11	
NC_Zn03	$SrFe_{12}O_{19}/Co_{0.7}Zn_{0.3}Fe_2O_4$	0.31	
NC_Zn05	$SrFe_{12}O_{19}/Co_{0.5}Zn_{0.5}Fe_2O_4$	0.53	

The powder samples were characterized using a Bruker D8 Advance diffractometer (solid state rapid LynxEye detector, Cu Kα radiation, Bragg–Brentano geometry, DIFFRACT plus software) in the 10°–140° 2θ range with a step size of 0.013° (counting time was 4 s per step). Rietveld analysis was performed on the X-ray powder diffraction (XRPD) data using the FULLPROF program [25]. The diffraction peaks were described by a modified Thompson-Cox-Hastings pseudo-Voigt function. A peak asymmetry correction was made for angles below 40° (2θ). Background intensities were estimated by interpolating between up to 60 selected points. A NIST LaB_6 660b standard was measured under the same conditions as the samples to account for the instrumental contribution to the peak broadening.

Transmission electron microscopy (TEM) analysis was carried out using a Philips CM200 microscope operating at 200 kV and equipped with a LaB_6 filament. For TEM observations, the samples, in form of powder, were prepared using the following procedure. A small quantity of powder was dispersed in ethanol and subjected to ultrasonic agitation for approximately one minute. A drop of the suspension was deposited on a commercial TEM grid covered with a thin carbon film. Finally, the grid was kept in air until complete ethanol evaporation.

Magnetic measurements were performed at room temperature using a Quantum Design superconducting quantum interference device (SQUID) magnetometer, which can supply a maximum field of 5 T. Isothermal field-dependent magnetization loops were recorded by sweeping the field in the − 5 T to + 5 T range. To get information about the irreversible processes, direct current demagnetization (DCD) remanence curves were measured by applying a progressively higher DC reverse field to a sample previously saturated under a field of −5T and by recording, for each step, the value of the remanent magnetization, which was then plotted as a function of the reverse field [26]. To avoid any displacement and preferential orientation of the crystallites under the external magnetic field during measurement, the nanopowders were immobilized with a glue in appropriate capsules (no significant magnetic contribution from the glue was observed during the measurements).

3. Results and discussion

The development of hard/soft bi-magnetic composites at the nanoscale is very challenging, owing to the various parameters that must be considered when they are synthesized, such as morpho-structural features of the hard and soft phases, quality of the interphase between materials and the ease as well as the reproducibility of the synthesis [2,3]. In our previous results, we were able to assess the efficiency of the sol–gel technique in the realization of such nanocomposites (NCs) [12,14,15,17,18,24]. In this regard, we first adopted this chemical approach to couple two different magnetic phases to design improved magnetic NCs, consisting of a hard SFO phase magnetically coupled to a softer CFO phase. The ratio was fixed to SFO/CFO 80/20 w/w % as a model system to investigate the Zn doping of CFO and its effect on morphological and magnetic properties of NCs. The XRPD pattern of NC after the thermal treatment is shown in Fig. 1a (black curve). All the reflections can be ascribed to the hexagonal structure typical of strontium hexaferrite (indicated in black), with space group $P6_3/mmc$ [27]; on the other hand, the reflections of the CFO phase are not clearly visible, because of their low intensity and the overlapping with more intense reflections of SFO phase. The characteristic reflections (200), (311),(400), (511) and (440) (in green) can be indexed as a spinel (Fd-3 m) [9]. In particular, the latter reflection is a clear confirmation of the presence of CFO phase, as it is not overlapping with any of the reflections

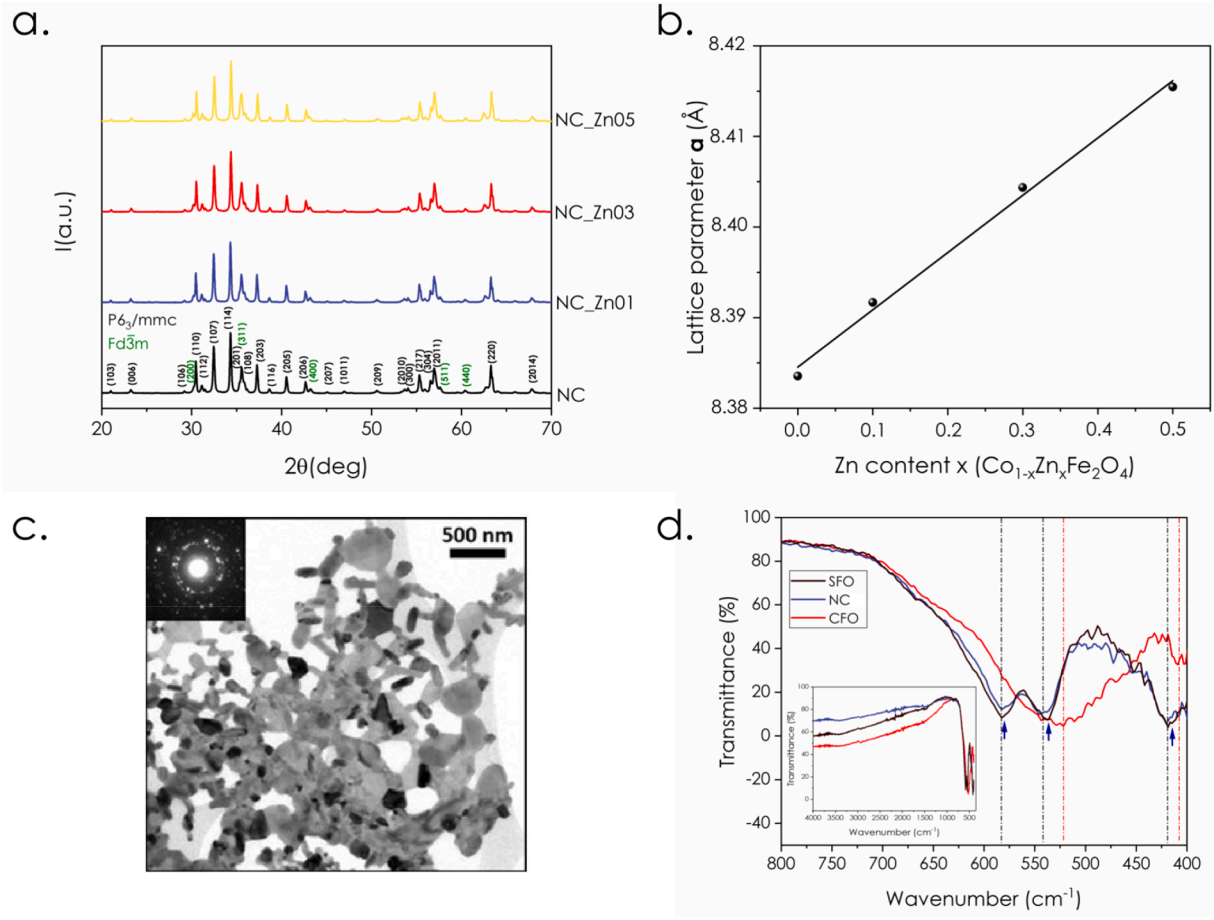

Fig. 1. (a) XRPD patterns of NC and NC$_s$_Zn, including (b) lattice parameters as a function of Zn^{2+}amount; (c) TEM general view of NC and corresponding SAED pattern (inset); (d) FTIR spectra for NC and the individual members SFO and CFO as a reference [18].

of SFO. Rietveld analysis was performed to extract the lattice parameters (see Table 2). Since the values for both phases are in a very good agreement with the reference values [24,27,28], and no peak shift is observed in the pattern, we can reasonably assume that the two phases are well crystallized, without undergoing any evident diffusion. All the doped NC$_s$_Zn samples (Fig. 1a) can be indexed as a combination of cubic spinel Fd-3 m and hexagonal P6$_3$/mmc structures, as for NC. It is noteworthy that no reflections ascribable to other phases were observed in the patterns, confirming that the inclusion of Zn^{2+} does not induce the formation of secondary phases. Interestingly, the lattice parameters (shown in Table 2) for CFO phase increase with the content of Zn^{2+}, confirming its inclusion in the cubic structure, which induces the expansion of unit cell, as reported in literature [7,22,29]. While in contrast, SFO lattice parameters are in perfect agreement with reference values, confirming the preferential inclusion of zinc in CFO, with respect to SFO, with no evident diffusion despite the high annealing temperature. The actual stoichiometries were checked by ICP-AES, confirming the amount of metal cations in the composites, within the experimental error. The obtained mean crystallite size (see Table 2) is equal, within experimental error in all the samples, indicating that change of stoichiometry in cobalt ferrites does not significantly affect morphological feature of the samples. A typical TEM bright field image of NC is reported in Fig. 1c. The sample is formed by irregular platelets interconnected to form porous aggregates. Selected area electron diffraction (SAED) measurements have revealed that all the visible diffraction spots can be associated to the SFO and CFO phases, no other phases have been detected, confirming what observed by XRPD (see the inset of Fig. 1c). Moreover, FTIR revealed to be a useful tool to give some qualitative information about the composition of NC, with respect to the individual phases, as the Me–O (Me = Co, Fe) stretching modes of ferrites fall in the fingerprint range[22]. The spectra are shown in Fig. 1d. The metal–oxygen stretching modes of the octahedral and tetrahedral sites for SFO appear in the 400–450 cm^{-1} and 530–600 cm^{-1} ranges respectively (indicated by the black dashed lines arrows) [30]. Their appearance is highlighted in the NC (blue arrows), also showing a slight redshift towards CFO values. Consistently, the metal–oxygen stretching modes of CFO fraction are overlapping and the intensity too low to be distinguished. The composition was confirmed by ICP. To explain the effect of the introduction of the soft phase in the hard-magnetic matrix, a field-dependent magnetization loop for NC was acquired and reported in Fig. 2a. The M vs H curve reaches the saturation at high fields, so the M_S values can be evaluated at 5 T (all the parameters are reported in

Table 2
Lattice parameters (a, b, and c), average crystallite sizes for CFO (<d >) and along ab and c planes for SFO (d_{ab} and d_c, respectively) extracted from Rietveld refinement (uncertainties in the last digit are given in parenthesis).

Id	SFO		CFO	d_{ab} (nm)	d_c (nm)	$<d>^{CFO}$ (nm)
	a = b (Å)	c (Å)	a = b = c (Å)			
NC	5.88069 (1)	23.04252 (9)	8.38354 (7)	85 (7)	60(4)	35(2)
NC_Zn01	5.88029 (2)	23.04203 (7)	8.39167 (8)	89(6)	66(6)	40(2)
NC_Zn03	5.88004 (2)	23.04199 (9)	8.40437 (7)	80(7)	58(5)	40(3)
NC_Zn05	5.88008 (2)	23.04271 (9)	8.41546 (9)	77(8)	60(4)	39(3)

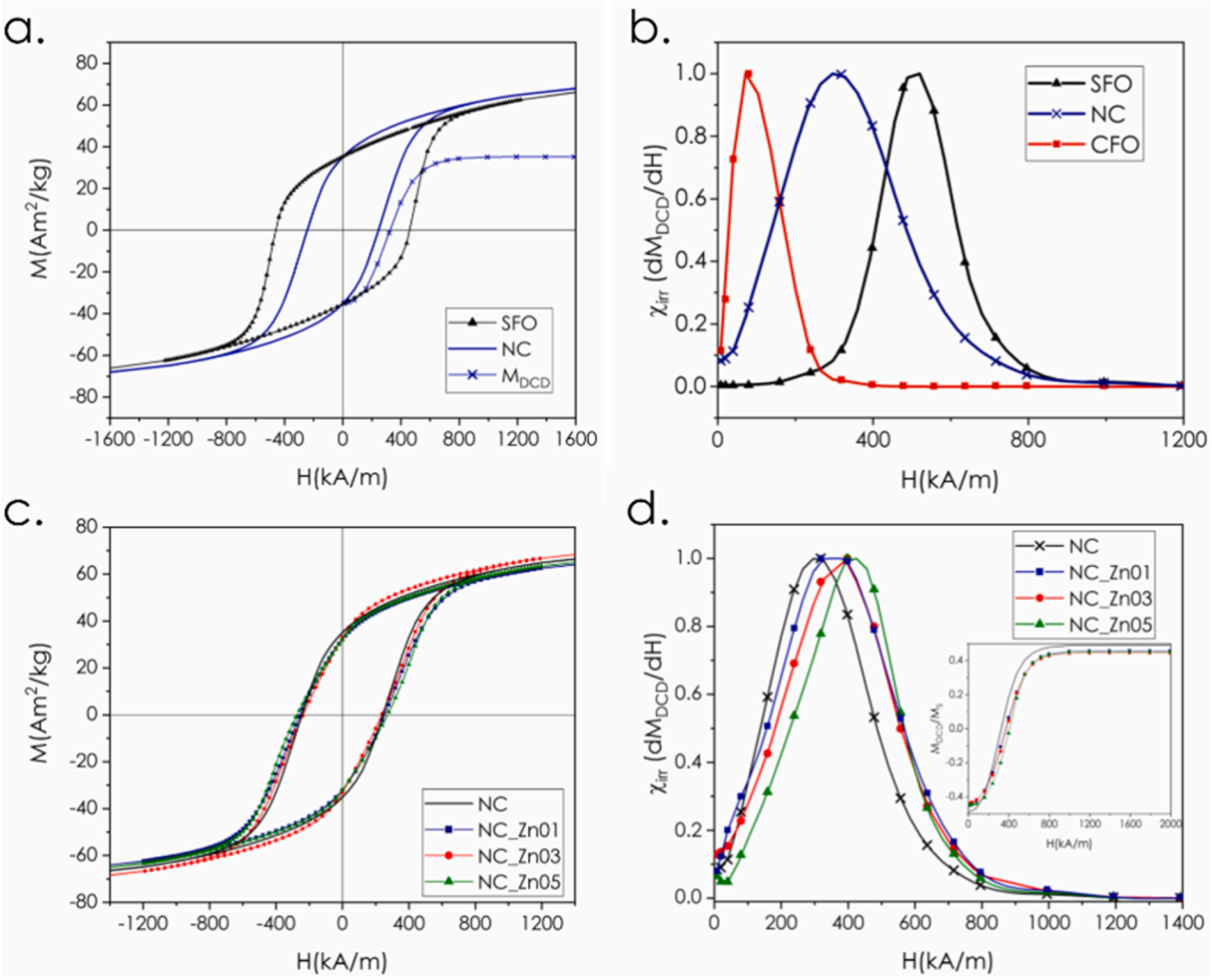

Fig. 2. (a) Magnetization M vs. magnetic field H curves for SFO and NC, and M_{DCD} for NC; (b) normalized irreversible susceptibility χ_{irr} vs reverse magnetic field H curves of NC and the individual SFO and CFO phases (data for SFO and CFO from [18]); (c) M vs. H curves and (d) normalized χ_{irr} vs H curves for NC and NCs_Zn at 300 K; the inset shows the reduced M_{DCD} vs H.

Table 3
Saturation magnetization (M_S), reduced remanence magnetization (M_R/M_S), coercive field (H_C) and average switching field, extracted from SFDs, (H_{SW}) of NC and NCs_Zn measured at 300 K. Data for SFO [18] is added for comparison.

Id	M_S^{5T} (Am²/kg)	M_R/M_S	H_C (kA/m)	H_{SW} (kA/m)
SFO	69.9 (5)	0.50	463(5)	520(5)
NC	71.8(4)	0.49	250(3)	306(2)
NC_Zn01	70.1(4)	0.46	251(5)	353(6)
NC_Zn03	74.0(3)	0.45	240(7)	376(4)
NC_Zn05	71.2(4)	0.45	265(5)	410(6)

Table 3). NC unambiguously exhibits a single reversal process of magnetization, suggesting that the two magnetic phases are homogeneously dispersed and strongly coupled, owing to the efficiency of the one-pot sol–gel method. In a previous study [24], we reported for comparison the magnetic properties of a physically mixed sample (NC_{MIX}) , showing instead an hysteresis loop typical of weakly coupled systems [14]. NC shows an intermediate magnetic behaviour between the two individual SFO and CFO phases [24], in good agreement with the limit of exchange-coupling [1]. To better highlight the presence of exchange-coupling interaction, we have performed additional direct current demagnetization (DCD) experiments [31]: the first order differentiated curves of M_{DCD} with respect to H (switching field distributions, or SFDs) are displayed in Fig. 2b, from which we proved that NC present a strong contribution, centered at a single field that can be attributed to the reversal process of unique assemblies, intermediate between the two individual phases (SFO and CFO), while perfect coupling leads to magnetic softening resulting in an exchange-coupled system. This evidences that our synthesis approach resulted in a magnetically coupled system, where a strong coupling is promoted by the proper nanosized texture [18]. To explore the possible effects of tuning the magnetic performance of such composite, our strategy is to tailor the magnetic anisotropy (and subsequently the softness) of the CFO phase by the simple replacement of metal cations, specifically Co^{2+}, partially with the diamagnetic Zn^{2+}. CFO is expected to show an inverse spinel structure, $[Fe^{3+}]_{Td}[Co^{2+},Fe^{3+}]_{Oh}O_4$: Zn^{2+} preferentially occupies tetrahedral Td sites, inducing the partial migration of Td Fe^{3+} ions to octahedral ones Oh [22]. This suggests that the antiferromagnetic coupling among Fe^{3+} ions in Td and Oh sites is lowered, and M_S increases up to a threshold value, above which the ferrimagnetic order is destabilized by the weakening of the exchange interaction between Td and Oh sites [7,22]. We point out that the purpose here is not to perform a systematic tuning of the magnetic anisotropy of CFO by Zn-doping, which has already been reported in earlier publications [7,22]. Rather, our aim is to show the feasibility of the one-pot synthesis method in tailoring the magnetic properties of the soft phase in an efficient and simple way by elemental doping, and hence the resulting performance of the NCs. To evaluate the effect on the magnetic properties, field-dependent magnetization loops at 300 K for NCs_Zn were investigated: Fig. 2c shows that all the curves exhibit a unique reversal process of magnetization, with variations in the extrinsic properties, as reported in

Table 3: the M_S is expected to increase when Zn^{2+} increases in the CFO phase, contributing to the average M_S in the composite. This is true up to a threshold value, that in our case is 0.3, which is similar to the values reported in literature for samples prepared with a similar method [7], but slightly higher, probably because of the very high annealing temperature, leading to more crystalline particles, with modified cationic distribution [20]. This matches the XRPD data supporting the occupation of Td sites by zinc. Then M_S starts to decrease in good agreement with literature [20,32]. The behaviors displayed by M_R and H_C are slightly more complex. It is noteworthy that the M_R/M_S is decreasing with Zn content, according to Table 3. This might be ascribed to a decrease of super-exchange interaction between Td and Oh sites in CFO structure with the increase of Zn content, leading to a decrease of remanence of the soft phase. Additionaly, the H_C values for NCs show no evident change, in spite of the substitution of Co^{2+} with Zn^{2+}, which promotes a decrease of H_C, owing to the decrease of magnetic anisotropy of the soft phase. Interestingly, the SFDs for doped NCs, shown in Fig. 2d, exhibit a single reversal process of magnetization, indicating the strong interphase coupling. Furthermore, we point out that the adopted synthetic approach allowed the soft grains to preserve the nanometric size despite the drastic annealing conditions, keeping its crystallite sizes around the critical stable single-domain size for CFO (~40 nm) [33]. Therefore, we assume that the effective coupling arises from a strong exchange-interaction between the two components, which stems from the overall homogeneous dispersion of small grains of the soft phase into the hard SFO matrix. Despite the good results in terms of magnetic coupling, the decrease of the remanence with respect to the starting NC, makes this kind of composite unsuited for realizing PMs. Nevertheless, we provide evidence of successful exchange-coupling interaction in hard-soft composites at the nanoscale, showing the feasibility of the sol–gel approach in synthesizing nanocomposites with complex stoichiometry, and also the tunability of the magnetic performance that can be achieved by chemical engineering.

4. Conclusion

In summary, we have shown that sol–gel synthesis is a reliable and simple way to design bi-magnetic nanocomposites, obtaining direct exchange-interaction. XRPD, TEM, and SQUID magnetometry suggest that the single reversal process is due to the optimized dispersion of the particles in NC, owing to the control over the size/distribution achievable in this morphology. We have explored the possibility to finely tune the magnetic properties of the softer phase, by introducing Zn^{2+}. From XRPD we have evidence of its inclusion in the CFO lattice. The increase of zinc amount has a non-monotonical effect on the overall M_S of the nanocomposites, with a maximal value of ~ 74 Am^2/kg for $Zn^{2+} = 0.3$, owing to the replacement of Co^{2+} that induces a rearrangement in the magnetic structure. Our results support the conclusion that the synthesis method strongly affects the cation distribution in the spinel structure of CFO, and demonstrate the suitability of this approach to obtain systems with a high degree of exchange-coupling as well as control the magnetic properties of the final designed nanocomposites.

Declaration of Competing Interest

The authors declare that they have no known competing financial interests or personal relationships that could have appeared to influence the work reported in this paper.

Acknowledgements

We thank the Swedish Energy Agency (project number 46561-1) and Swedish Research Council (VR) for financially supporting this work. TS acknowledges financial support from VR (starting grant No. 2017-05030). We are grateful to Dr. Francesco Soggia for the technical support provided during the preparation and the analysis of the samples by ICP-AES at the Università di Genova.

References

[1] R. Skomski, P. Manchanda, P.K. Kumar, B. Balamurugan, A. Kashyap, D. J. Sellmyer, Predicting the future of permanent-magnet materials, IEEE Trans. Magn. 49 (7) (2013) 3215–3220, https://doi.org/10.1109/TMAG.2013.2248139.
[2] B. Balamurugan, D.J. Sellmyer, G.C. Hadjipanayis, R. Skomski, Prospects for nanoparticle-based permanent magnets, Scr. Mater. 67 (6) (2012) 542–547, https://doi.org/10.1016/j.scriptamat.2012.03.034.
[3] E.E. Fullerton, J.S. Jiang, S.D. Bader, Hard/soft magnetic heterostructures: model exchange-spring magnets, J. Magn. Magn. Mater. 200 (1-3) (1999) 392–404, https://doi.org/10.1016/S0304-8853(99)00376-5.
[4] J.M.D. Coey, Hard magnetic materials: a perspective, IEEE Trans. Magn. 47 (12) (2011) 4671–4681, https://doi.org/10.1109/TMAG.2011.2166975.
[5] J.M.D. Coey, Magnetism and Magnetic Materials, Cambridge University Press, 2001. https://doi.org/10.1017/CBO9780511845000.
[6] E.F. Kneller, R. Hawig, The exchange-spring magnet: a new material principle for permanent magnets, IEEE Trans. Magn. 27 (4) (1991) 3588–13560, https://doi.org/10.1109/20.102931.
[7] A. Omelyanchik, K. Levada, S. Pshenichnikov, M. Abdolrahim, M. Baricic, A. Kapitunova, A. Galieva, S. Sukhikh, L. Astakhova, S. Antipov, B. Fabiano, D. Peddis, V. Rodionova, Green synthesis of Co-Zn spinel ferrite nanoparticles: magnetic and intrinsic antimicrobial properties, Materials (Basel). 13 (2020) 5014, https://doi.org/10.3390/ma13215014.
[8] S. Eriksson, P. Eklund, Effect of magnetic properties on performance of electrical machines with ferrite magnets, J. Phys. D. Appl. Phys. 54 (5) (2021) 054001, https://doi.org/10.1088/1361-6463/abbfc5.
[9] C. Granados-Miralles, A. Quesada, M. Saura-Múzquiz, H.L. Andersen, J. F. Fernández, M. Christensen, Expanding the tunability and applicability of exchange-coupled/decoupled magnetic nanocomposites, Mater. Chem. Front. 4 (4) (2020) 1222–1230, https://doi.org/10.1039/C9QM00713J.
[10] P. Jenuš, M. Topole, P. McGuiness, C. Granados-Miralles, M. Stingaciu, M. Christensen, S. Kobe, K. Žužek Rožman, A. Belik, Žužek Rožman, Ferrite-based exchange-coupled hard-soft magnets fabricated by spark plasma sintering, J. Am. Ceram. Soc. 99 (6) (2016) 1927–1934, https://doi.org/10.1111/jace:14193.
[11] L. Pan, D. Cao, P. Jing, J. Wang, Q. Liu, A novel method to fabricate $CoFe_2O_4$/$SrFe_{12}O_{19}$ composite ferrite nanofibers with enhanced exchange coupling effect, Nanoscale Res. Lett. 10 (2015) 131, https://doi.org/10.1186/s11671-015-0829-z.
[12] G. Muscas, P. Anil Kumar, G. Barucca, G. Concas, G. Varvaro, R. Mathieu, D. Peddis, Designing new ferrite/manganite nanocomposites, Nanoscale 8 (4) (2016) 2081–2089, https://doi.org/10.1039/C5NR07572F.
[13] H. Zeng, J. Li, J.P. Liu, Z.L. Wang, S. Sun, Exchange-coupled nanocomposite magnets by nanoparticle self-assembly, Nature 420 (6914) (2002) 395–398, https://doi.org/10.1038/nature01208.
[14] F. Sayed, G. Muscas, S. Jovanovic, G. Barucca, F. Locardi, G. Varvaro, D. Peddis, R. Mathieu, T. Sarkar, Controlling magnetic coupling in bi-magnetic nanocomposites, Nanoscale 11 (30) (2019) 14256–14265, https://doi.org/10.1039/C9NR05364F.
[15] F. Sayed, G. Kotnana, G. Muscas, F. Locardi, A. Comite, G. Varvaro, D. Peddis, G. Barucca, R. Mathieu, T. Sarkar, Symbiotic, low-temperature, and scalable synthesis of bi-magnetic complex oxide nanocomposites, Nanoscale Adv. 2 (2) (2020) 851–859, https://doi.org/10.1039/C9NA00619B.
[16] G. Kotnana, F. Sayed, D.C. Joshi, G. Barucca, D. Peddis, R. Mathieu, T. Sarkar, Novel mixed precursor approach to prepare multiferroic nanocomposites with enhanced interfacial coupling, J. Magn. Magn. Mater. 511 (2020) 166792, https://doi.org/10.1016/j.jmmm.2020.166792.
[17] T. Sarkar, G. Muscas, G. Barucca, F. Locardi, G. Varvaro, D. Peddis, R. Mathieu, Tunable single-phase magnetic behavior in chemically synthesized $AFeO_3$ –MFe_2O_4 (A = Bi or La, M = Co or Ni) nanocomposites, Nanoscale 10 (48) (2018) 22990–23000, https://doi.org/10.1039/C8NR06922K.
[18] P. Maltoni, T. Sarkar, G. Barucca, G. Varvaro, F. Locardi, D. Peddis, R. Mathieu, Tuning the magnetic properties of hard-soft $SrFe_{12}O_{19}$ /$CoFe_2O_4$ nanostructures via composition/interphase coupling, J. Phys. Chem. C. 125 (10) (2021) 5927–5936, https://doi.org/10.1021/acs.jpcc.1c0035510.1021/acs.jpcc.1c00355.s001.
[19] R.C. Pullar, Hexagonal ferrites: a review of the synthesis, properties and applications of hexaferrite ceramics, Prog. Mater. Sci. 57 (7) (2012) 1191–1334, https://doi.org/10.1016/j.pmatsci.2012.04.001.
[20] M. Albino, E. Fantechi, C. Innocenti, A. López-Ortega, V. Bonanni, G. Campo, F. Pineider, M. Gurioli, P. Arosio, T. Orlando, G. Bertoni, C. de Julián Fernández, A. Lascialfari, C. Sangregorio, Role of Zn2+ Substitution on the Magnetic, Hyperthermic, and Relaxometric Properties of Cobalt Ferrite Nanoparticles, J. Phys. Chem. C. 123 (2019) 6148–6157. https://doi.org/10.1021/acs.jpcc.8b10998.
[21] J. Fischbacher, A. Kovacs, M. Gusenbauer, H. Oezelt, L. Exl, S. Bance, T. Schrefl, Micromagnetics of rare-earth efficient permanent magnets, J. Phys. D. Appl. Phys. 51 (19) (2018) 193002, https://doi.org/10.1088/1361-6463/aab7d1.
[22] V. Mameli, A. Musinu, A. Ardu, G. Ennas, D. Peddis, D. Niznansky, C. Sangregorio, C. Innocenti, N.T.K. Thanh, C. Cannas, Studying the effect of Zn-substitution on the magnetic and hyperthermic properties of cobalt ferrite nanoparticles, Nanoscale 8 (19) (2016) 10124–10137, https://doi.org/10.1039/C6NR01303A.
[23] G. Muscas, S. Jovanović, M. Vukomanović, M. Spreitzer, D. Peddis, Zn-doped cobalt ferrite: tuning the interactions by chemical composition, J. Alloys Compd. 796 (2019) 203–209, https://doi.org/10.1016/j.jallcom.2019.04.308.

[24] P. Maltoni, T. Sarkar, G. Varvaro, G. Barucca, S.A. Ivanov, D. Peddis, R. Mathieu, Towards bi-magnetic nanocomposites as permanent magnets through the optimization of the synthesis and magnetic properties of $SrFe_{12}O_{19}$ nanocrystallites, J. Phys. D Appl. Phys. 54 (12) (2021) 124004, https://doi.org/10.1088/1361-6463/abd20d.

[25] J. Rodríguez-Carvajal, Recent advances in magnetic structure determination by neutron powder diffraction, Phys. B Condens. Matter. 192 (1-2) (1993) 55–69, https://doi.org/10.1016/0921-4526(93)90108-I.

[26] D. Peddis, P.E. Jönsson, S. Laureti, G. Varvaro, Magnetic Interactions, in: C. Binns (Ed.), Front. Nanosci., Elsevier, 2014: pp. 129–188. https://doi.org/10.1016/B978-0-08-098353-0.00004-X.

[27] X. Obradors, X. Solans, A. Collomb, D. Samaras, J. Rodriguez, M. Pernet, M. Font-Altaba, Crystal structure of strontium hexaferrite SrFe12O19, J. Solid State Chem. 72 (2) (1988) 218–224, https://doi.org/10.1016/0022-4596(88)90025-4.

[28] M. Popescu, C. Ghizdeanu, Cation distribution in cobalt ferrite-aluminates, Phys. Status Solidi 52 (2) (1979) K169–K172, https://doi.org/10.1002/(ISSN)1521-396X10.1002/pssa:v52:210.1002/pssa:2210520259.

[29] J.-T. Jang, H. Nah, J.-H. Lee, S. Moon, M. Kim, J. Cheon, Critical enhancements of MRI contrast and hyperthermic effects by dopant-controlled magnetic nanoparticles, Angew. Chemie Int. Ed. 48 (7) (2009) 1234–1238, https://doi.org/10.1002/anie.200805149.

[30] V. Harikrishnan, R. Ezhil Vizhi, A study on the extent of exchange coupling between $(Ba_{0.5}Sr_{0.5}Fe_{12}O_{19})_{1-x}(CoFe_2O_4)_x$ magnetic nanocomposites synthesized by solgel combustion method, J. Magn. Magn. Mater. 418 (2016) 217–223, https://doi.org/10.1016/j.jmmm.2016.03.037.

[31] A. López-Ortega, M. Estrader, G. Salazar-Alvarez, A.G. Roca, J. Nogués, Applications of exchange coupled bi-magnetic hard/soft and soft/hard magnetic core/shell nanoparticles, Phys. Rep. 553 (2015) 1–32, https://doi.org/10.1016/j.physrep.2014.09.007.

[32] G. Barrera, M. Coisson, F. Celegato, S. Raghuvanshi, F. Mazaleyrat, S.N. Kane, P. Tiberto, Cation distribution effect on static and dynamic magnetic properties of $Co_{1-x}Zn_xFe_2O_4$ ferrite powders, J. Magn. Magn. Mater. 456 (2018) 372–380, https://doi.org/10.1016/j.jmmm.2018.02.072.

[33] C.N. Chinnasamy, B. Jeyadevan, K. Shinoda, K. Tohji, D.J. Djayaprawira, M. Takahashi, R.J. Joseyphus, A. Narayanasamy, Unusually high coercivity and critical single-domain size of nearly monodispersed $CoFe_2O_4$ nanoparticles, Appl. Phys. Lett. 83 (14) (2003) 2862–2864, https://doi.org/10.1063/1.1616655.